Magnetic actuation of microparticles for mass transfer enhancement

Philip A. LISK[1], Erell BONNOT[1], Md. Taifur RAHMAN[2], Farid AIOUACHE[3], Robert BOWMAN[4], Robert POLLARD[4], Evgeny REBROV[1,2*]

* Corresponding author: Tel.: ++44 (0)24 765 22202; Email: e.rebrov@warwick.ac.uk
[1]School of Chemistry and Chemical Engineering, Queen's University Belfast, Belfast, UK
[2]School of Engineering, University of Warwick, Coventry, UK
[3]School of Engineering, Lancaster University, UK
[4]School of Mathematics and Physics, Queen's University Belfast, Belfast, UK

Abstract:

The motion of magnetic microparticles (250μm diameter) in a circular microfluidic reactor with a diameter of 10 mm under time dependent magnetic field has been studied using CFD code COMSOL. The effect of actuation protocol on the local and average particle velocity has been investigated. The local Sh numbers were obtained as a function of angular particle position in the range of Re numbers between 0.05 and 10 while the particle velocity was changed over two orders of magnitude. Under time dependent magnetic field, the thickness of the boundary layer continuously changes which results in an increased mass transfer towards the particle surface under periodic particle velocity conditions as compared to steady state velocity conditions. A good agreement between numerical and experimental data has been observed.

Keywords: Microparticles, magnetic actuation, particle motion dynamics.

1. Introduction

Magnetic microparticles (MMPs) are of great interest in the field of microfluidics. Their high specific surface area, chemical compatibility and ease of external manipulation allows for applications in many microfluidic systems[1]. Under an externally applied magnetic field, MMPs can be agitated to improve mixing of chemical/material entities in fluidic channels and microreactors otherwise limited by external diffusion[2,3]. The agitated MMPs traverse the fluid of interest enabling surface contact with chemical entities in the bulk fluid and enhancing mixing through momentum transfer of the particle itself.

As a result, there has been a large amount of research into MMP manipulation using various actuation techniques. A system of multi-planar permanent magnets acting with a time varied electromagnet has demonstrated improved particle control with long structured chains of magnetic particles[4]. Dynamic feedback control of magnetic particles has achieved defined particle motion[5,6]. In spite of the several experimental studies that are available in recent literature, numerical analysis of MMP motion has been sparse. Previously particle

motion in gradient magnetostatic fields has been investigated by Carol et al.[7]. These authors studied particle motion under different actuation protocols and observed enhanced mass transfer rates at higher particle velocities. Enhanced mass transfer to the particle surface was also observed under oscillatory flow conditions around a rigid sphere[8].

In this study, numerical simulations of single particle motion in a circular reactor under a time dependent magnetic field have been performed. The trajectories of a MMP under the influence of magnetic and hydrodynamic forces have been obtained. The effect of periodic changes in particle velocity on mass transfer rate to the particle surface has been investigated. The numerical results have been compared with experimental data.

2. Experimental Method

The experimental set up, designed for MMP manipulation consisted of four iron bars 14cm long, cross section 2.5 x 2.5 cm^2 connected to four coils. The coils coupled in pairs were connected to two separate DC power supplies by a conductive iron base, shown in Figure 1. Sinusoidal voltages

were applied through the electromagnets producing magnetic fields varying with angular frequency (ω), voltage (V) and phase shift (φ):

$$V_1 = V_{01} \cdot \sin(\omega t) \qquad (1)$$
$$V_2 = V_{02} \cdot \sin(\omega t + \varphi) \qquad (2)$$

where V_1 and V_2 are the applied voltages through both pairs of magnets separated by a phase shift φ.
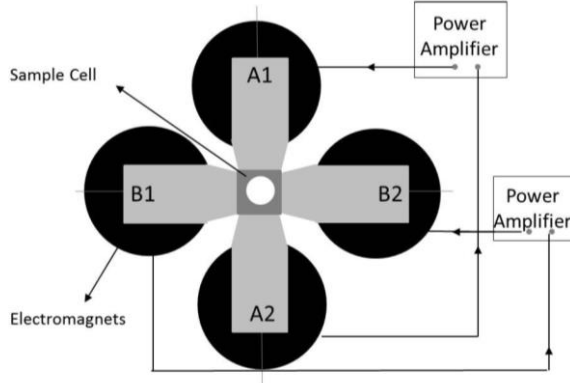

Figure 1: Schematic view of the magnetic actuation system.

The PDMS (polydimethylsiloxane) circular reactor cell was fabricated for this study using a standard soft lithography method (diameter: 10 mm, depth: 0.5 mm). The cell was firstly filled with acetonitrile and loaded with magnetic microparticles (impregnated with ferrite-based magnetic nanoparticles) before being positioned in the middle of the magnetic actuation system. Voltages (25-100V) were applied through the magnets and particle trajectories were recorded using an optical microscope (Leica M165FC) connected to a high speed video camera (Leica DFC310 FX) with a resolved pixel size of 6.5 x 6.5μm². Images were taken at a frame rate of 20 fps and analyzed using the NI Vision Software.

3. Numerical Modelling

Two numerical models were created with the aim of replicating experimental conditions within the microreactor. The first model was used to obtain the particle trajectories between of four iron electromagnets of 14×2 cm² surrounding the circular reactor (Fig. 2). Magnetic and hydrodynamic forces were simulated using a system of governing equations. Firstly, the applied field through the magnets was calculated in terms of the magnetic flux density **B**, vector potential **A** and magnetization **M,** Eqs. 3-5.

$$\sigma \frac{\partial \mathbf{A}}{\partial t} + \nabla \times (\mu_0{}^{-1} \mu_r{}^{-1} \mathbf{B}) - \sigma \boldsymbol{v} \times \mathbf{B} = J_e \qquad (3)$$

$$\sigma \frac{\partial \mathbf{A}}{\partial t} + \nabla \times (\mu_0{}^{-1} \mathbf{B} - \mathbf{M}) - \sigma \boldsymbol{v} \times \mathbf{B} = J_e \qquad (4)$$

$$\boldsymbol{B} = \nabla \times \mathbf{A} \qquad (5)$$

Particle motion, dictated by changing magnetic field gradients is defined using the magnetophoretic force $\boldsymbol{F_m}$ (6).

$$\boldsymbol{F_m} = 2\pi r_p{}^3 \mu_0 \mu_r k \nabla \boldsymbol{H}^2 \qquad (6)$$

Here $\boldsymbol{F_m}$ is calculated in terms of particle radius (r_p), permeability of free space (μ_0), relative permeability (μ_r), ratio of magnetic susceptibility (k) and the gradient of the magnetic field($\nabla \boldsymbol{H}$). Secondly, hydrodynamic forces acting on the MMPs were defined. Particle velocity (**v**) throughout the fluid medium is hindered by the viscous drag force($\boldsymbol{F_d}$).

$$\boldsymbol{F_d} = 6\pi \mu r_p \boldsymbol{v} \qquad (7)$$

The viscous drag force acting on a spherical particle is given in terms of fluid viscosity (μ), particle radius (r_p) and particle velocity ($\boldsymbol{v}$).

A 250 μm particle was positioned into the centre of the reactor containing a fluid of equivalent of properties to that of acetonitrile (density 780 kg m⁻³ and viscosity 0.343 mPa.s). Magnetophoretic mobility of the particle was specified using the relative magnetic susceptibility (χ) of the particle, taken from VSM data.

Boundary conditions at the surrounding circular reactor wall were specified using the bounce wall condition which is defined using the particle velocity (**v**) and particle impact velocity (**v_c**).

$$\mathbf{v} = \mathbf{v_c} - 2(\mathbf{n}.\,\mathbf{v_c})\mathbf{n} \qquad (8)$$

Mesh specifications were focused on the central reactor. For particle motion considerations, a custom fluid dynamics mesh was used specifying the maximum and minimum element size to be 1.0×10^{-4} and 2.0×10^{-5} m respectively. Surrounding mesh refinements were carried out, specifying increased resolution for magnet faces and surrounding reactor boundaries.

Typical magnetic field distribution in the reactor is shown in Figure 2. The areas of highest magnetic flux density (in red) are observed around the perimeter of the reactor due to the pulling-force

towards the surrounding magnet faces.

The effect of non-uniform particle velocity on mass transfer was investigated in a separate model. The flow field around the fixed particle was simulated by the Navier-Stokes and the continuity equations for incompressible flow (9-10). Subsequently the convection diffusion equations in the bulk fluid were solved (11).
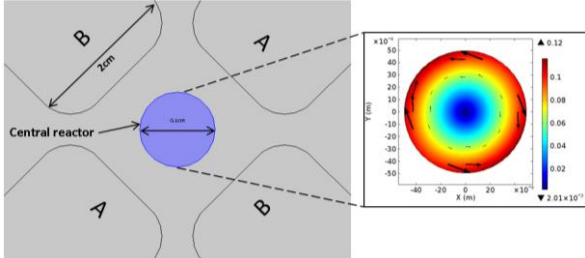
Figure 2: Geometry of computational domain, showing typical magnetic field distribution in central cell in terms of surface magnetic flux density **B** (T) (colour spectra) and gradient of the magnetic field squared ∇H^2 (arrow surface plot).

$$\rho(\mathbf{u}.\nabla)\mathbf{u} = \nabla.\left[-\text{PI} + \mu\left(\nabla\mathbf{u} + (\nabla\mathbf{u})^T\right)\right] + \mathbf{F} \qquad (9)$$

$$\rho\nabla.\mathbf{u} = 0 \qquad (10)$$

$$\frac{\partial c_i}{\partial t} + \nabla.(D_i\nabla c_i + \mathbf{u}c_i) = 0 \qquad (11)$$

A fast first order reaction was simulated on the outer surface of the particle assuming zero concentration of the reactant on the particle surface. The reaction rate (**R**) on the particle surface was defined by Eq **12.**

$$R = k_c\,A_p\,C_A \qquad (12)$$

where k_c is the mass transfer coefficient, A_p is the particle surface area and C_A is the reactant bulk concentration.

Geometry and boundary conditions for the physical model are shown in Fig 3. No slip conditions were specified on the surface of the particle and surrounding walls. Pulsating flow was simulated by applying a sine function to the inlet velocity with an amplitude from 0.1 to 10 times the average velocity (v_{av}). The mass transfer coefficient was also calculated in the range of constant flow velocities between 0.1 and 10 mm s^{-1}.

4. Results and discussion

Simulated particle positions under time dependent magnetic field are shown in Figure 4a for magnetic
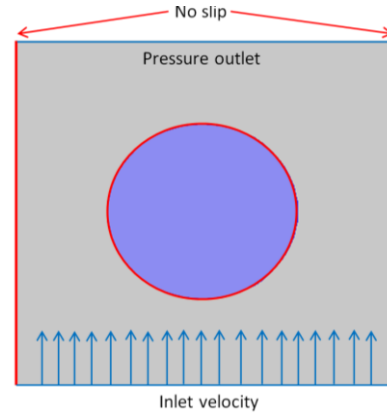
Figure 3: Schematic view of physical geometry of the second model, Fluidic boundary conditions included for particle and surrounding walls.

field frequencies of 0.1, 0.3 and 0.6 Hz. It can be seen that the particle moves near the perimeter of the reactor at all operating frequencies. Similar trajectories were observed experimentally (Fig 4b).
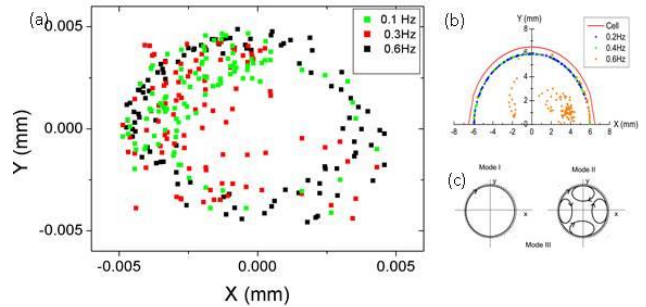

Figure 4: (a) simulated particle positions for a time interval of 50 s, (b) experimental particle positions for a time interval of 50 s, (c) schematic view of characteristic particle trajectories.

However simulated particle trajectories demonstrated larger scattering as compared to the experimental ones. Much larger reactor coverage was observed at each frequency under simulated conditions. Two modes of particle motion were identified (Fig 4c). At frequencies below 0.4 Hz, particle motion follows a circular path along the reactor wall as the particles experience the highest magnetic field gradient towards the surrounding magnets. At frequencies above 0.4Hz, circular motion around the cell is interrupted by a few oscillation cycles between the nearest magnetic pole and the centre of the reactor. At higher frequencies of the magnetic field, the particles could not follow the path of the highest gradient of magnetic field. As a result they follow different trajectories resulting in several cycles of oscillations near the individual magnetic poles. This results in greater reactor coverage.

The local particle velocity was obtained from the particle trajectories (Fig 5). It can be seen that

during a single period of rotation in the reactor, the particle experiences four acceleration and deceleration phases. The absolute value of particle velocity changes over an order of magnitude between 0.1 and 2.0 mm s^{-1}.
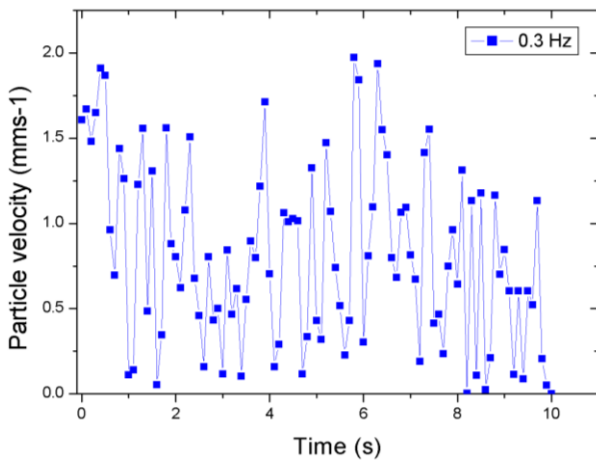
Figure 5: Simulated local particle velocities under a sinusoidal magnetic field with a frequency of 0.3 Hz.

The second numerical model was used to study mass transfer rate of reactant A to the surface of the particle at several flow conditions. In this model, the particle was fixed and the fluid velocity was changed in accordance to the particle velocity values obtained from the first model (Fig 5). Figure 6 shows concentration distribution near the reactive surface where a fast chemical reaction takes place. The thickness of the mass transfer boundary layer depends on the angular position.
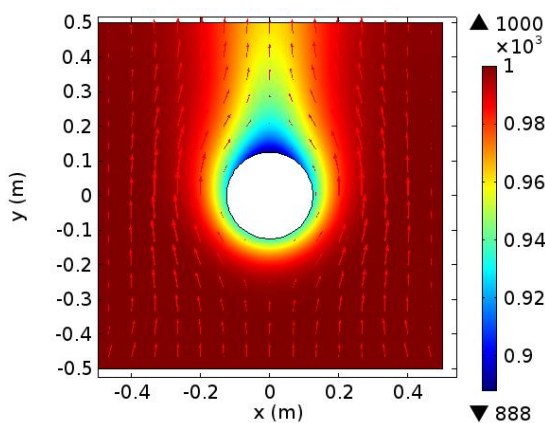
Figure 6: The concentration profile of reactant A (mol m^{-3}) over a 250 µm particle under constant flow conditions.

The mass transfer rate was calculated as a function of angular position around the surface of the particle for two flow conditions representing (i) actual motion of the particle with a frequency of 0.1 Hz and an average velocity of 0.1mm s^{-1} and

(ii) steady state flow conditions (Fig 7). In the latter case, the numerical solution matches the exact solution for the local Sh number around the sphere.
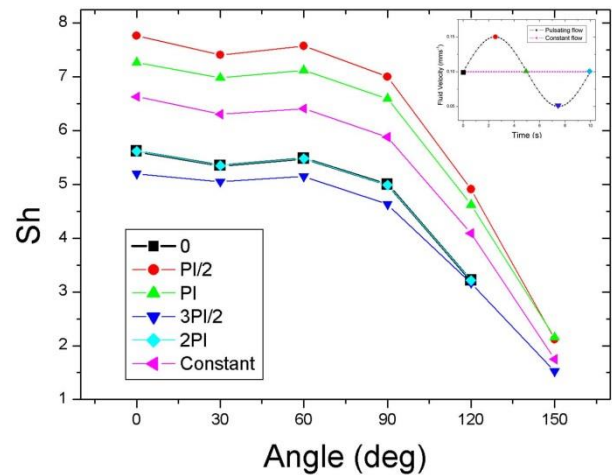
Figure 7: Local Sherwood number (Sh) as a function of angular position around a circular particle at different cycle times during the motion of a magnetic particle with a frequency of 0.1 Hz and an average velocity of 0.1 mm s^{-1}. Steady state Sherwood number is shown for comparison for the same average velocity.

When the motion resembles that of a magnetic particle under the time dependent magnetic field, the average Sherwood number was found to be 5.181 as compared with 5.178 for constant flow velocity. As the average flow rate increases, the mass transfer rate progressively decreases under periodic flow conditions as compared to the constant velocity case.

5. Conclusions

The trajectories of a 250 µm magnetic microparticle have been numerically investigated under a time dependent magnetic field created with a quadrupole arrangement of electromagnets. During a single period of rotation in the reactor, the particle experiences four acceleration and deceleration phases. The absolute value of particle velocity changes over an order of magnitude between 0.1 and 2.0 mm s^{-1}. This results in different mass transfer rate to the particle surface as compared to constant fluid flow conditions. As the average flow rate increases, the mass transfer rate progressively decreases under periodic movement conditions.

References

1. van Reenen, A., de Jong, A.M., den Toonder, J.M.J., Prins. M.W.J. 2014. Integrated lab-on-chip biosensing systems based on magnetic particle actuation – a comprehensive review, **14**, 1966-1986.

2. Gijs, M.A.M. 2004. Magnetic bead handling on-chip: new opportunities for analytical applications. *Microfluid. Nanofluidics*, **1**, 22–40.

3. Lee, S.H., van Noort, D., Lee, J.Y, Zhang, B.T., Park, T.H. 2009. Effective mixing in a microfluidic chip using magnetic particles. *Lab Chip* **9,** 479–482.

4. Gao, Y., van Reenen, A., Hulsen, M.A., de Jong, A.M., Prins, M.W.J., den Toonder, J.M.J. 2013. Chaotic fluid mixing by alternating microparticle topologies to enhance biochemical reactions. *Microfluid. Nanofluidics* **16,** 265–274.

5. Probst, R., Lin, J., Komaee, A., Nacev, A., Cummins, Z., Shapiro, B. 2011. Planar steering of a single ferrofluid drop by optimal minimum power dynamic feedback control of four electromagnets at a distance. *J. Magn. Magn. Mater.* **323,** 885–896.

6. Zhang, Z., Huang, Y., Member, S. 2010. Actively Controlled manipulation of a magnetic microbead using quadrupole magnetic tweezers. **26,** 531–541.

7. Veeramachaneni, U.K., Carroll, R.L. 2009. Analysis of forces acting on superparamagnetic beads in fluid medium in gradient magnetic fields governing equations. Proceedings of the COMSOL Conference. Boston.

8. Blackburn, H.M. 2002. Mass and momentum transport from a sphere in steady and oscillatory flows. *Phys. Fluids* **14,** 3997.